# Chapter 1

# Introduction

*In this chapter, we provide an overview of the Sun and Sun-like stars, focusing on their structure, magnetic activity, and energetic phenomena such as flares and superflares. The discussion begins with the fundamental aspects of the Sun, including its internal structure, energy transport mechanisms, and atmosphere. The role of the solar dynamo in driving the Sun's magnetic activity cycle is also explored. Since the Sun is not unique in exhibiting such magnetic activity, the focus then shifts to Sun-like stars, detailing their stellar dynamo processes, the generation of large-scale magnetic fields, and how these fields contribute to the occurrence of energetic events similar to those observed in the solar atmosphere. The chapter then delves into the nature of stellar magnetic activities and their diverse manifestations across different layers of a stellar atmosphere, observable in a wide range of wavelengths. Particular emphasis is placed on understanding transient magnetic phenomena such as flares and coronal mass ejections, which serve as key diagnostics of the stellar magnetic energy release and variability. The chapter further discusses both observational signatures and theoretical*

***models that describe the underlying mechanisms driving these energetic transient plasma processes.***

Stars are the fundamental building blocks of galaxies, playing a crucial role in the structure and evolution of the universe. However, stars are spatially unresolved, meaning their surface and atmospheric features cannot be directly observed in greater detail. The Sun, our nearest star, is an exception—it is the only star that can be spatially resolved, allowing us to study its surface and atmospheric phenomena with high precision. Advanced space-borne observations, such as the Solar Dynamics Observatory (SDO), Solar and Heliospheric Observatory (SOHO), Interface Region Imaging Spectrograph (IRIS), Aditya-L1, etc., provide highly detailed observations of the solar activity, including flares, sunspots, and coronal mass ejections. Given the wealth of information available about the Sun, it serves as a crucial reference for understanding other stars. By applying the solar analogy, we can develop theories and models to study stellar magnetic activities across various Sun-like stars, making the Sun an essential benchmark for astrophysical research. Conversely, the diverse population of Sun-like stars also provides evolutionary context for deciphering the Sun's past and future magnetic behavior. The overview of the Sun, its various layers, and its magnetism is presented in Section 1.1.

## 1.1 Overview of the Sun

The Sun, our closest G2-type main-sequence star, is Earth's primary energy source and plays a vital role in sustaining life. It significantly influences Earth's climate and space weather, making its study essential for understanding stellar behavior and cosmic plasma dynamics. As a massive sphere of plasma, the Sun maintains stability by balancing its gravitational pull and the outward pressure from internal energy production, a state known as hydrostatic equilibrium. Its composition consists mainly of 92% Hydrogen

atoms, 8% Helium atoms by number, and nearly 0.1% of heavier elements such as carbon, nitrogen, and oxygen. Some physical parameters of the Sun are given in Table 1.1. With a surface temperature of approximately 5,800 K, the Sun is positioned in the middle of the Hertzsprung-Russell diagram, as shown in Fig. 1.1. It is about 4.5 billion years old, currently in the hydrogen-burning phase of its life cycle. Being a plasma body, the Sun is structured into distinct layers, which are broadly categorized into its interior and atmospheric (or exterior) layers. These layers have different physical properties and different mechanisms responsible for the energy transport. A brief overview of these layers is provided below.

Table 1.1: Physical parameters of the Sun (Credit: Priest 2014; Srivastava et al. 2024)

| Physical Parameters | Value |
|---|---|
| Age | 4.6 billion years |
| Mass (M⊙) | $1.99 \times 10^{30}$ kg |
| Radius (R⊙) | $6.955 \times 10^{8}$ m |
| Luminosity (L⊙) | $3.86 \times 10^{33}$ erg $s^{-1}$ |
| Photospheric temperature | 5785 K |
| Mean distance from earth | 1AU ($1.496 \times 10^{11}$ m) |
| Mass-loss rate | $10^{9}$ kg $s^{-1}$ |
| Spectral type | G2V |
| Synodic rotation period | ~ 26.24 days (at equator) |
| Sidereal rotation period | ~ 24.47 days (at equator) |

### 1.1.1 The Solar Interior

The interior of the Sun contains the core layers (center at 0 to 0.25 R⊙), the radiative zone (approximately 0.25 to 0.7 R⊙), and the convection zone (approximately 0.7 to 1 R⊙) as shown in Fig. 1.2. Different physical processes are dominant in these layers. The core is the region where thermonuclear fusion occurs, primarily through the proton-proton chain, converting hydrogen into helium while releasing energy in the form of X-rays, gamma rays (26.2 Mev), and neutrinos (0.5 Mev) (Cox et al., 1991). Due to its high temperature

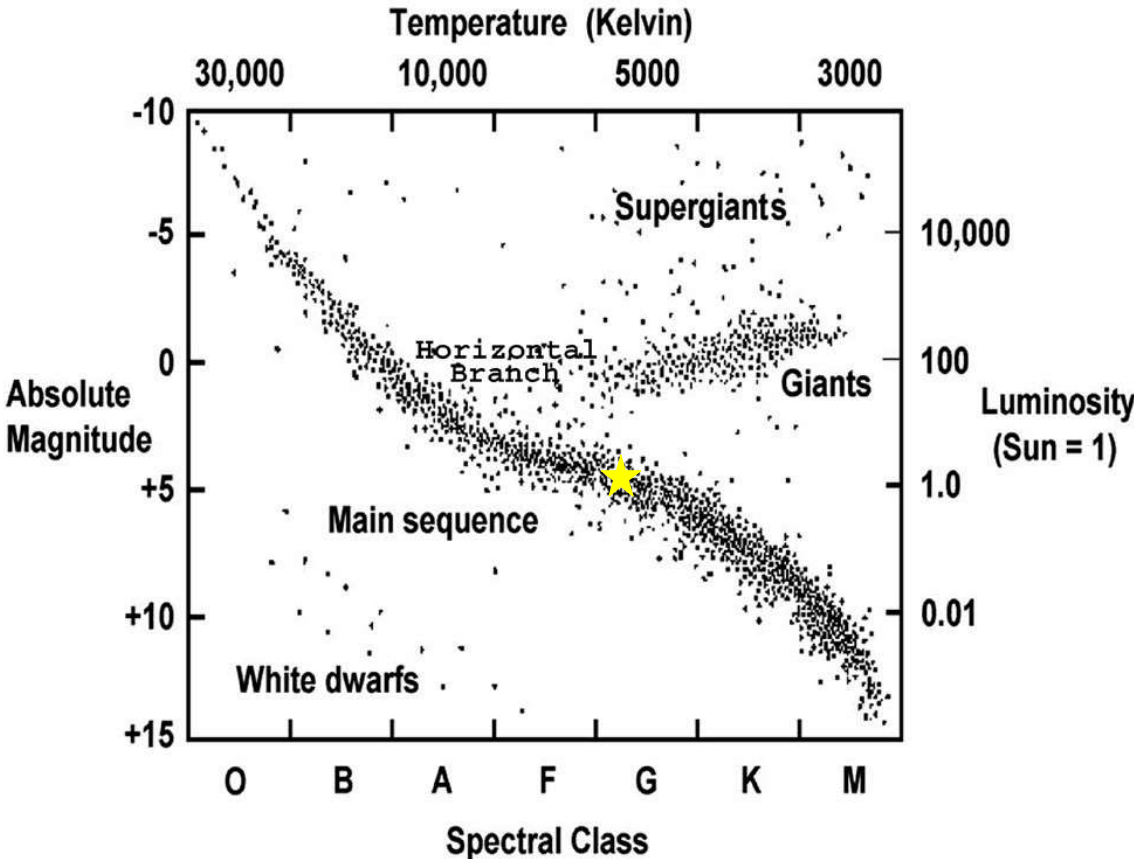


Figure 1.1: The Hertzsprung–Russell (H–R) Diagram for stars in the solar neighbourhood, illustrating the relationship between stellar absolute magnitude, spectral class, temperature, and luminosity. A yellow star symbol marks the location of the Sun, highlighting its position on the main sequence. (Image Credit: Chandra X-ray Observatory, NASA/CXC)

of about 15 MK, the core is the most energetic part of the Sun, generating 99% of its total energy, even though it accounts for only about one-fourth of the solar radius (Carroll and Ostlie, 2006). The energy produced in the core moves outward into the radiative zone, where energy is transported primarily via radiative diffusion. Here, photons undergo multiple scattering interactions with surrounding particles, causing a random walk effect that delays their journey toward the surface for about $10^5$ to $10^6$ years. As photons move outward, the temperature gradually drops from 15 MK to about 1.5 MK at the base of the convective zone. At the boundary between the radiative and convective zones lies the tachocline, a thin but significant transition layer where the Sun's differential rotation

begins (Spiegel and Zahn, 1992). This region is believed to play a crucial role in the solar magnetic field generation due to strong rotational shear, leading to the formation of the solar dynamo. Beyond this, the convective zone is characterized by the turbulent convective motions, where energy is transported through the movement of plasma. As the plasma cools, the recombination of electrons and ions increases opacity, making radiation inefficient for energy transport, and convection takes over. Large-scale convective currents form granules and supergranules, visible as the specific patterns on the solar photosphere. The temperature in this zone decreases from 2 MK to about 5,800 K at the surface. The convective zone plays a crucial role in shaping solar magnetic activity, as the rising and twisting plasma drives the emergence of sunspots, solar flares, and coronal mass ejections (CMEs). The dynamic interaction between convection and magnetic fields governs many of the Sun's observable surface and atmospheric phenomena, influencing space weather and solar cycles.

### 1.1.2 The Solar Atmosphere

The solar atmosphere consists of four main layers: the photosphere, chromosphere, transition region, and corona, each exhibiting distinct physical characteristics and playing a crucial role in the generation of energetic dynamical plasma processes. The photosphere is the visible surface layer of the Sun, where most of the Sun's radiation is emitted. This layer has a temperature range of 3,800 K to 6,600 K and a density of approximately $10^{17}$ $cm^{-3}$ (Priest, 1982). It contains dynamic features such as sunspots, which are regions of the strong magnetic fields (1–3 kG) (Phillips, 1995), and supergranulation, which arises from the convective motions. The next layer, the chromosphere, extends about 2,500 km above the photosphere, with temperatures rising from 5,800 K to ~25,000 K (Carroll and Ostlie, 2006). It is characterized by a complex and dynamic structure with features such as bright spicules (jet-like eruptions), dark filaments (large arcs of material), and prominences

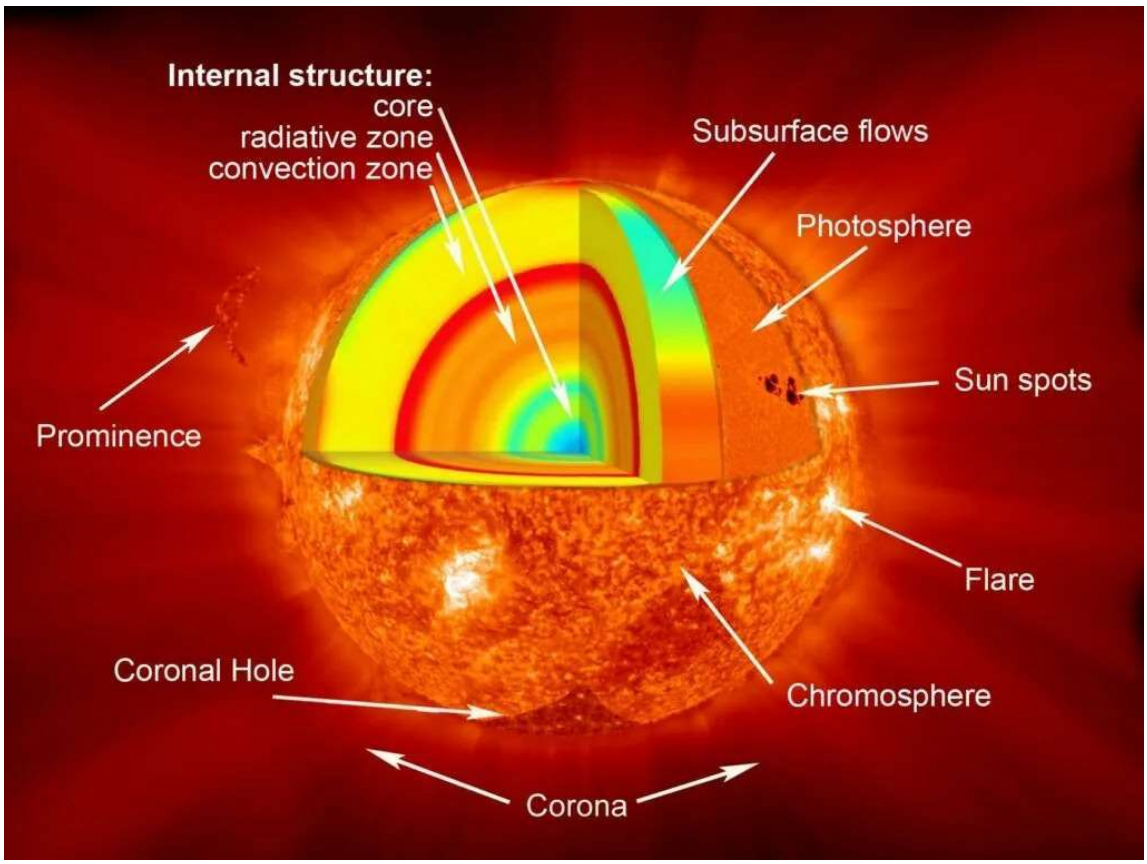


Figure 1.2: Structure of the Sun: A schematic representation of the Sun's internal and external layers. The solar interior consists of the core, where nuclear fusion occurs, followed by the radiative zone and the convective zone. The solar atmosphere comprises with the photosphere, chromosphere, and corona. (Image Credit: NASA/Goddard)

(gigantic plumes of gas). The chromosphere emits ultraviolet and optical wavelengths, including H$\alpha$ (656.28 nm) and Ca II K (393.37 nm) lines, allowing many solar features to be observed in this prominent spectral range.

The transition region lies above the chromosphere. It is a very thin (~100 km) layer where temperature increases sharply from ~20,000 K to a few million K (Judge, 2008). In this region, gas pressure drops exponentially while magnetic pressure decreases more gradually, leading to plasma beta ($\beta$) < 1, where the magnetic fields dictate the plasma motions (Mariska, 1992). The corona, an outermost layer of the solar atmosphere, extends far into interplanetary space. It is highly structured, consisting of loops, streamers, and

plumes that are shaped by the Sun's magnetic fields (Aschwanden and Nightingale, 2005). The corona was first observed during a total solar eclipse, appearing as a faint halo surrounding the Sun. Compared to the bright photosphere, the coronal brightness is nearly $10^{-6}$ times fainter, decreasing further with distance (Rosner et al., 1978a). Despite its low density ($10^8$ - $10^9$ cm$^{-3}$), the corona is extremely hot, with temperatures reaching several million Kelvin, a phenomenon still not fully understood and known as the Coronal Heating Problem. Unlike the expectation of decreasing temperature with distance from the Sun, the temperature rapidly increases from 5,800 K in the photosphere to $\sim 10^6$ K in the corona within just a few tens of kilometers (see Fig. 1.3). This layer is optically thin in the visible wavelengths, making direct observations difficult. However, with the space-based telescopes, the corona can be observed in X-rays and Extreme Ultraviolet (EUV), revealing its intricate magnetic structures. Another crucial feature originating from the corona is the solar wind, a continuous flow of charged particles that extends throughout the heliosphere. The slow solar wind moves at $\sim$ 440 km/s, while high-speed streams originating from coronal holes can exceed 1,000 km/s at 1 AU (Tu et al., 2005). These winds play a significant role in shaping space weather and influencing planetary environments. These atmospheric phenomena are linked with the Sun's magnetic field, the origin and evolution of which are understood through the framework of solar dynamo theory.

### 1.1.3 Solar Dynamo and Activity Cycle

In the early 20th century, Hale (1908) identified the magnetic nature of sunspots and their link to the solar activity cycle, laying the foundation for our understanding of solar magnetism. Subsequent magnetographic mappings of the Sun's surface revealed cyclic variations in the solar activity, regulating phenomena such as sunspots, solar flares, and coronal mass ejections (CMEs). These variations follow a well-defined pattern, with activity peaking at the solar maximum and declining at the solar minimum. This cyclic

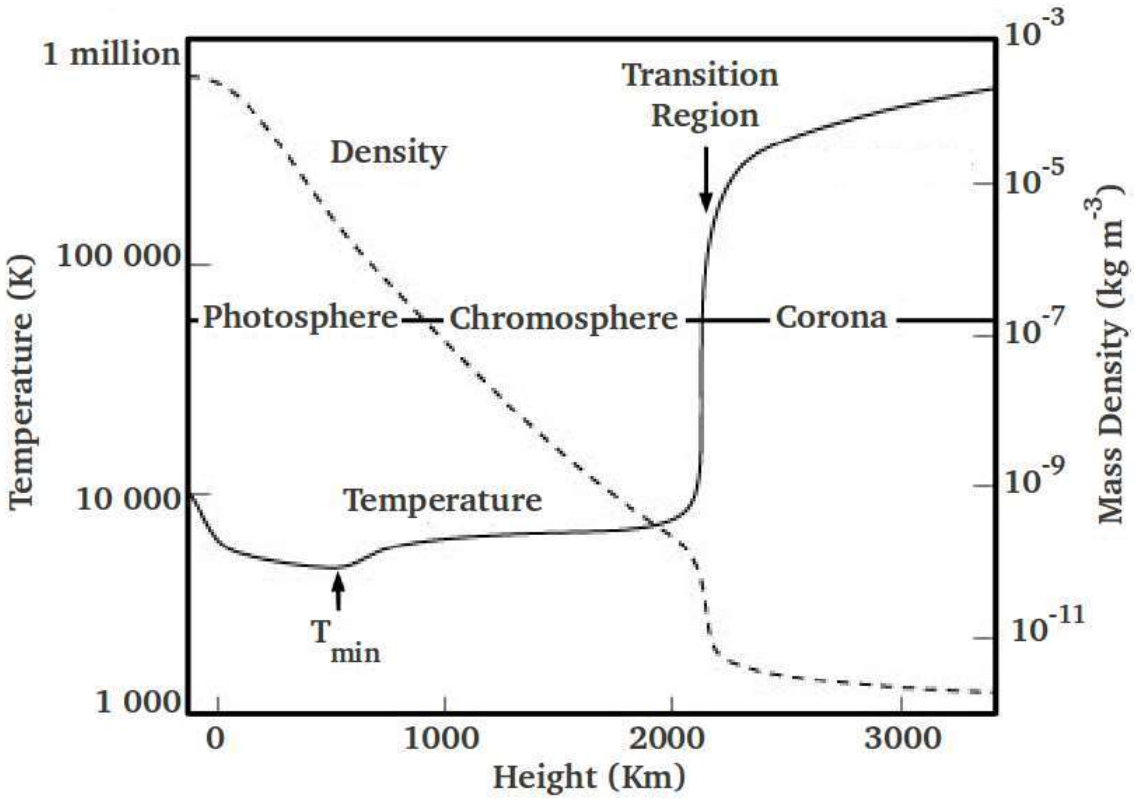


Figure 1.3: The temperature and density variations across different heights or layers of the solar atmosphere. (Image Credit: Kenneth R. Lang (2010))

behavior is explained by the $\alpha$–$\Omega$ dynamo model, which describes the generation and evolution of the Sun's magnetic field. In this framework, the differential rotation of the Sun (the $\Omega$-effect) stretches the poloidal magnetic field—connecting the poles—into a toroidal structure aligned in the east-west direction. Simultaneously, the convective motions in the Sun's interior (the $\alpha$-effect) twist and regenerate the poloidal fields (Babcock, 1961; Leighton, 1964; Parker, 1955), as illustrated in Fig. 1.4. The tachocline, a shear layer at the base of the convection zone, plays a critical role in this process by amplifying and storing magnetic fields before they emerge as sunspots and magnetic loops. This region rotates nearly rigidly with a period of approximately 30 days. Further explaining the reversal of

the Sun's magnetic polarity is the Babcock–Leighton model, which attributes the poleward

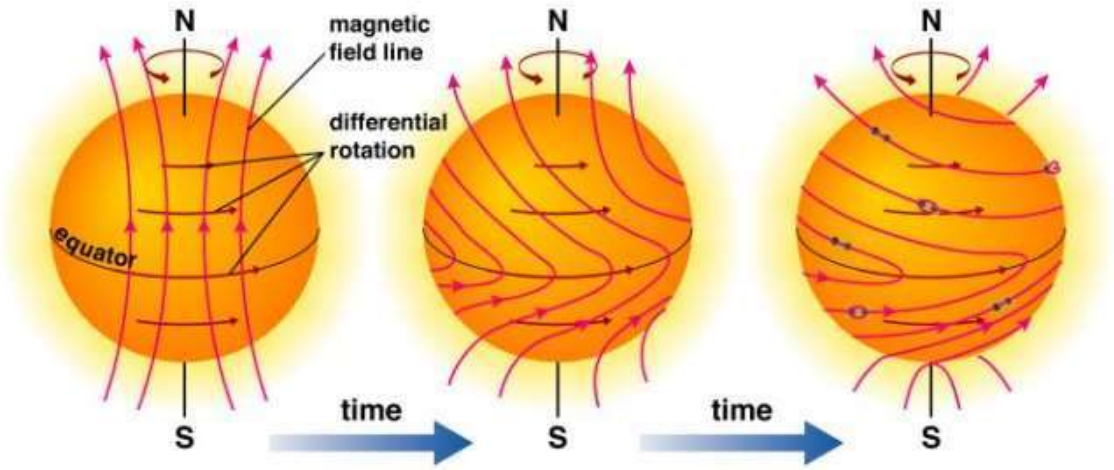


Figure 1.4: Schematic representation of the $\alpha$–$\Omega$ dynamo mechanism responsible for generating the solar magnetic field. Starting with a poloidal field (left image), which is transformed into a toroidal field through differential rotation (center image). This leads to the emergence of complex active regions (right image), and the cycle continues as convective motions regenerate the poloidal field. (Image Credit: Carroll and Ostlie (2006))

transport of magnetic flux to a meridional circulation, forming the characteristic butterfly diagram of the sunspot migration (Leighton, 1969). The $\alpha$-effect is also central to the formation of sunspot groups, as described by Joy's Law (Hale et al., 1919), where sunspot pairs appear tilted, with trailing spots located farther from the equator than the leading ones. Recent advancements in dynamo theory have focused on refining solar cycle models and exploring the magnetic field regeneration using magnetohydrodynamic simulations to reproduce the large-scale magnetic cycles (see Charbonneau, 2020).

This ongoing cycle of the transformation between poloidal and toroidal fields, as confirmed by magnetographic studies, forms the basis of the Sun's 11-year magnetic cycle and the 22-year Hale polarity cycle (Landstreet, 1992). Differential rotation continuously stretches and winds the surface magnetic field, leading to its fragmentation and poleward transport, ultimately converting the toroidal field back into a poloidal configuration. The

solar activity cycle is famously depicted in the butterfly diagram (see Fig. 1.5). The Sun's magnetic field, considerably stronger than planetary magnetic fields, is generated within the tachocline layer, where the field strengths can reach up to $10^5$ G. Magnetic flux tubes formed by buoyancy ascend through the convection zone, following convective instability described by the Schwarzschild criterion (Schwarzschild, 1906). Upon reaching the surface, these flux tubes give rise to active regions such as sunspots, which can have magnetic fields of around $10^3$ G, and coronal loops, which show strengths of about $10^2$ G at their photospheric footpoints, decreasing to around 10 G at coronal heights. The Section 1.2 now describes about Sun-like stars in the framework of stellar dynamo, rotation, and magnetic activity.

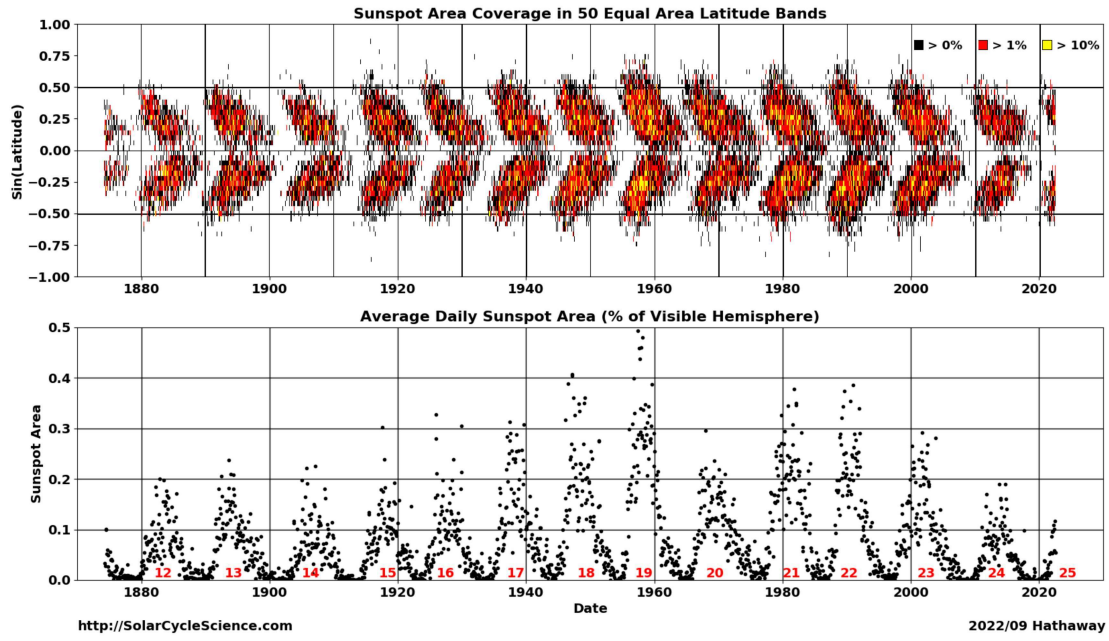


Figure 1.5: Butterfly diagram illustrating the migration of sunspots over the solar cycle, where sunspots first appear at higher latitudes and gradually shift toward the equator as the cycle progresses. The upper panel shows the distribution of the sunspot area as a function of latitude, where colors indicate the percentage of area coverage, and the lower panel shows the average daily sunspot area variation over time. (Image Credit: Hathaway (2022))

## 1.2 Sun-Like Stars

Sun-like stars are generally characterized by fundamental properties similar to those of the Sun, including mass, radius, surface temperature, chemical composition, and internal structure. However, distinctions exist among the terms "Sun-like," "solar-type," "solar analog," and "solar twin," depending on how closely they resemble the Sun. Solar-type stars have a broader classification, typically covering F, G, and K spectral types with masses ranging from 0.8 to 1.2 solar masses (Hall et al., 2007). While they share some general features with the Sun, they may differ significantly in age, activity, or elemental composition. Solar analogs are more precisely defined, having similar temperature, luminosity, and metallicity to the Sun, though variations in age and detailed abundance patterns may still exist. Solar twins, the most strictly defined category, exhibit nearly identical parameters to the Sun (do Nascimento et al., 2014). Although these terms are sometimes used interchangeably in astrophysics, this thesis adopts the term "Sun-like stars," similar to the solar-type stars within the spectral range F8–K2. These stars possess a radiative core and an outer convective envelope, which allows for the magnetic activity driven by an internal dynamo mechanism, much like the Sun.

A key question is why studying Sun-like stars is an important area of research. Investigating these stars provides insights into the Sun's past, present, and future activity, including its magnetic behavior, flare dynamics, and the potential for extreme events such as superflares. Understanding whether the Sun is capable of producing such powerful flares is crucial, as they could have significant consequences on Earth. Since direct solar records are insufficient, comparative studies with similar stars help to analyze extreme solar energetic particle events and stellar magnetic activity (Vasilyev et al., 2022). To explore these phenomena, it is essential to understand how magnetic fields are generated in these stars through the stellar dynamo process.

### 1.2.1 Stellar Dynamo Mechanisms

The generation of the stellar magnetic fields arises from the complex magnetohydrodynamic processes within the ionized plasma of stellar interiors. These fields are either measured directly through Zeeman effect (Landstreet, 1992) or inferred from the chromospheric and coronal emissions associated with the magnetic activity. In stars with radiative cores and convective envelopes—such as Sun-like stars, the magnetic fields are typically generated via an $\alpha$–$\Omega$ dynamo, a process similar to that operating in the Sun (as discussed in sub-section 1.1.3). However, the Sun alone cannot offer a complete picture of stellar dynamos across various stellar types and activity regimes. It is therefore essential to investigate other stars to understand how different internal structures, rotation rates, and convection properties influence the magnetic field generation.

Sun-like stars exhibit X-ray emissions from magnetically confined plasma at temperatures of several million Kelvin, similar to the Sun. However, their X-ray luminosities can reach up to $10^{32}$ erg s$^{-1}$, significantly exceeding the solar values by several orders of magnitude. This enhanced activity is largely attributed to their rapid rotation. Fast-rotating solar analogs experience stronger shear and enhanced Coriolis forces, which amplify both the $\alpha$ and $\Omega$ effects of the dynamo, making the magnetic field generation more efficient. Consequently, such stars host stronger toroidal magnetic fields, exhibit higher surface magnetic flux, and produce more frequent and energetic flares, including superflares. They also develop extensive and long-lived starspots, often much larger than sunspots. Observations show that these stars may have shorter or irregular magnetic cycles, contrasting with the Sun's regular 11-year cycle (Jeffers et al., 2023).

In contrast, fully convective, low-mass stars—lacking a tachocline layer—are believed to operate under a different dynamo regime, such as an $\alpha^2$ or $\alpha^2\Omega$ dynamo. Here, magnetic field generation is primarily driven by turbulent convection rather than differential rotation (Chabrier and Küker, 2006; Durney et al., 1993). Some simulations suggest that even weak

differential rotation in such stars can support large-scale, axisymmetric magnetic structures (Browning, 2008), indicating a spectrum of dynamo behaviors across different spectral types and masses.

### 1.2.2 Stellar Activity and Rotation Relation

Stellar dynamo theories predict that rotation plays a pivotal role in magnetic activity through $\alpha$–$\Omega$ or $\alpha^2$ mechanisms, with the $\alpha$-effect being essential in regenerating magnetic fields. Both models imply a positive correlation between rotation rate and the magnetic field strength (Browning et al., 2010), which directly affects observable activity indicators like X-ray luminosity (Pallavicini et al., 1981). Young, rapidly rotating stars tend to exhibit heightened magnetic activity, but this declines over the time as angular momentum is lost via magnetized stellar winds.

To better quantify this rotation-activity relation, researchers often use the Rossby number ($R_0 = P_{\rm rot}/\tau_c$), where $P_{\rm rot}$ is the rotation period and $\tau_c$ is the convective turnover time, the timescale for a convective cell to rise and fall within a fluid in the convection zone (Noyes et al., 1984b). The Rossby number provides a more accurate measure than rotation alone, as it incorporates the influence of stellar convection (Reiners, 2012). Studies of open clusters have shown that stars with moderate to slow rotation follow a trend where $L_X/L_{\rm bol} \propto R_0^{-2}$ (Randich, 2000). However, at high rotation rates ($R_0 \lesssim 0.1$), X-ray activity reaches a saturation limit of $L_X/L_{\rm bol} \sim 10^{-3}$ (Agrawal et al., 1986; Fleming et al., 1988; Pallavicini et al., 1990), beyond which further increases in rotation do not result in a stronger emission (see Fig. 1.6). This saturation threshold, first noted by Vilhu and Rucinski (1983) and Vilhu (1984), varies slightly with stellar parameters such as mass and spectral type.

Interestingly, ultra-fast rotators (e.g., $P_{\rm rot} < 1$ day) exhibit a decline in X-ray luminosity beyond the saturation threshold, a behavior termed "super-saturation" as shown in Fig. 1.6 Several hypotheses have been proposed to explain this phenomenon such as, saturation

of the internal dynamo (Vilhu and Walter, 1987), maximum surface coverage of active regions (Vilhu, 1984), magnetic flux concentration toward the poles (Solanki et al., 1997), and coronal stripping by centrifugal forces (Jardine and Unruh, 1999).

Overall, the activity–rotation relation provides a robust framework for understanding the evolution of magnetic activity in stars and highlights the influence of internal structure and rotation on stellar coronae. In Section 1.3, we elucidate various aspects of solar and stellar magnetic activities and their observational perspectives.

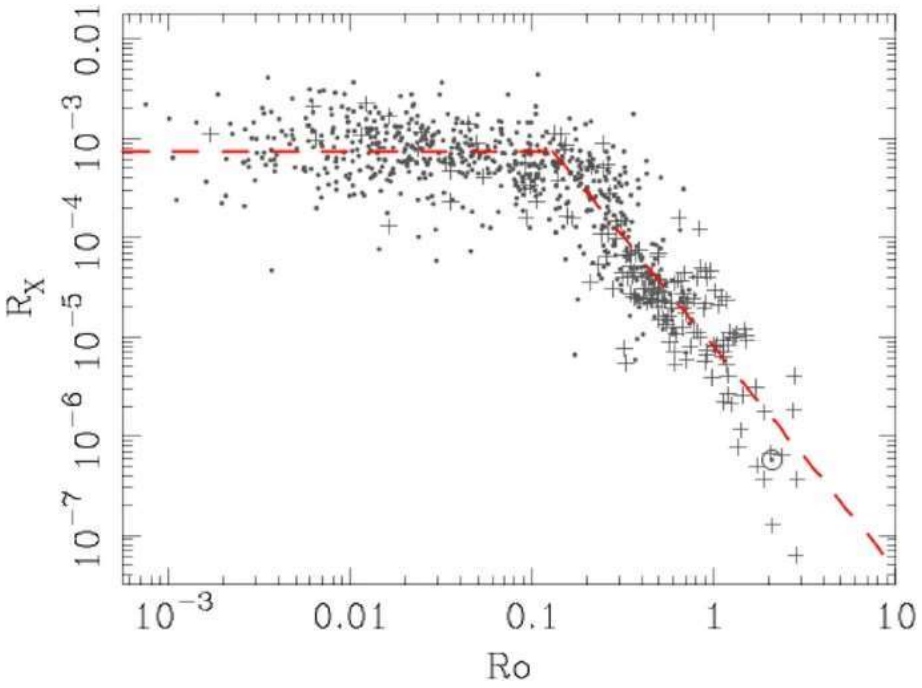


Figure 1.6: The ratio of X-ray to bolometric luminosity ($R_X = L_X/L_{\rm bol}$) is plotted against Rossby number ($R_0 = P_{rot}/\tau_c$). The red dashed line represents the best-fit activity–rotation trends in the saturated regime ($R_0 \leq 0.1$) and the non-saturated regime ($R_0 > 0.1$). (Image Credit: Wright et al. (2011))

## 1.3 Solar and Stellar Magnetic Activities

Magnetic fields generated by the stellar dynamo are fundamental in driving a variety of dynamic processes on the surfaces and in the atmospheres of the Sun and similar stars.

These magnetic activities manifest in various forms, some as long-lasting surface features such as starspots, and others as short-lived energetic events like flares, prominences, and coronal mass ejections (CMEs), triggered by the localized magnetic instabilities in the photosphere, chromosphere, and/or corona. These magnetic processes significantly influence the heating of stellar coronae and the overall structure of the stellar atmospheres. In this thesis, particular attention is given to the energetic events such as flares, superflares, and eruptions like CMEs. However, a broader overview of the magnetic activity in different layers of the solar and stellar atmospheres is also presented in the following sub-sections.

### 1.3.1 Photospheric Activities

Photospheric activity refers to the magnetic phenomena occurring in the visible surface layer of the Sun and similar Stars analogously. The dominant features include sunspots, faculae, granulation, and supergranulation as shown in Fig. 1.7. Among these, sunspots and their most likely stellar analogs, starspots, appear as dark, cooler regions caused by intense magnetic fields that inhibit convective heat transport. These features evolve over timescales of days to weeks and act as crucial indicators of surface magnetic activity. Starspots originate from magnetic flux tubes that penetrate the photosphere and extend into the upper atmosphere, forming magnetic loops with a dipolar structure. Based on the solar observations, sunspots consist of a darker central umbra, where strong vertical magnetic fields reduce convection, resulting in a temperature deficit of about 1700 K, surrounded by a somewhat warmer penumbra, where the magnetic field is more inclined and the temperature is lower by ~750 K with respect to the photospheric temperature (Berdyugina, 2005). Faculae, in contrast, are bright magnetic regions typically visible near the solar limb, where their contrast is enhanced. Though they also arise from magnetic activity, their field lines are more concentrated and localized than those in sunspots. Interestingly, during

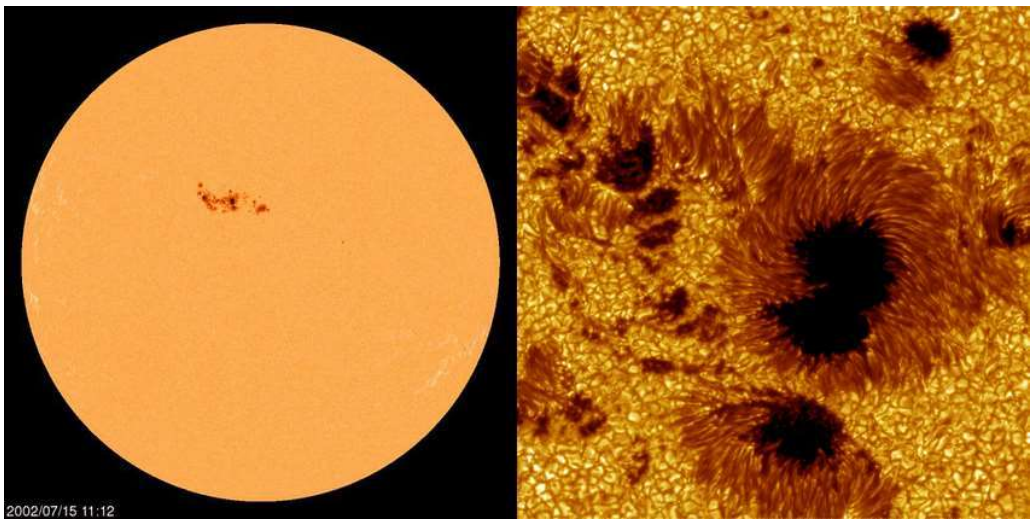


Figure 1.7: Left: Full-disk continuum image of active region captured by SOHO/MDI on July 15, 2002. Right: Enlarged view of the sunspot area, highlighting the umbra, penumbra, and surrounding granulation. (Image credit: SOHO [NASA & ESA], Royal Swedish Academy of Sciences)

the solar maxima, the brightening effect of faculae exceeds the dimming caused by the sunspots, leading to a slight net increase (~0.1%) in the solar brightness.

As dark starspots (cooler regions) rotate in and out of view due to the rotation of the star, they cause dips in the overall visible brightness of the star. These spots are cooler than the surrounding surface, so they emit less light, leading to a periodic variation in the optical light curve as shown in Fig. 1.8. This effect, first noted by Kron (1947) and later studied extensively by Hall (1976), provides a way to determine stellar rotation periods. The amplitude of these brightness variations depends on the size and contrast of the starspots (Strassmeier, 2009). In highly active stars, such as RS CVn binaries and young fast rotators, starspots can be orders of magnitude larger than those on the Sun (Strassmeier, 2009). Their presence leads to a significant periodic variation in the optical and X-ray emission. These variations have been well studied and documented using the long-term photometric and spectroscopic studies (Oláh et al., 2009; Vogt and Penrod, 1983). The Kepler mission has demonstrated that superflare-generating solar-type stars often show such rotational modulation, tightly linked to the longitudinal distribution of the large starspots (Notsu et al.,

2013). Additionally, the persistence of these large-scale starspots enables Doppler imaging techniques to reconstruct stellar surface maps, which is not feasible for the Sun due to the small size and rapid evolution of its sunspots.

Thus, while rotational modulation is a critical tool for studying magnetic activity in active stars, its impact on the Sun remains minimal, highlighting fundamental differences in stellar activity levels across different types of stars. In addition, some key observational tools, such as photometry, spectroscopy, and interferometry, along with diagnostic techniques like light curve modeling, Doppler imaging, and Zeeman Doppler imaging, play a crucial role in detecting and characterizing starspots and other photospheric features.

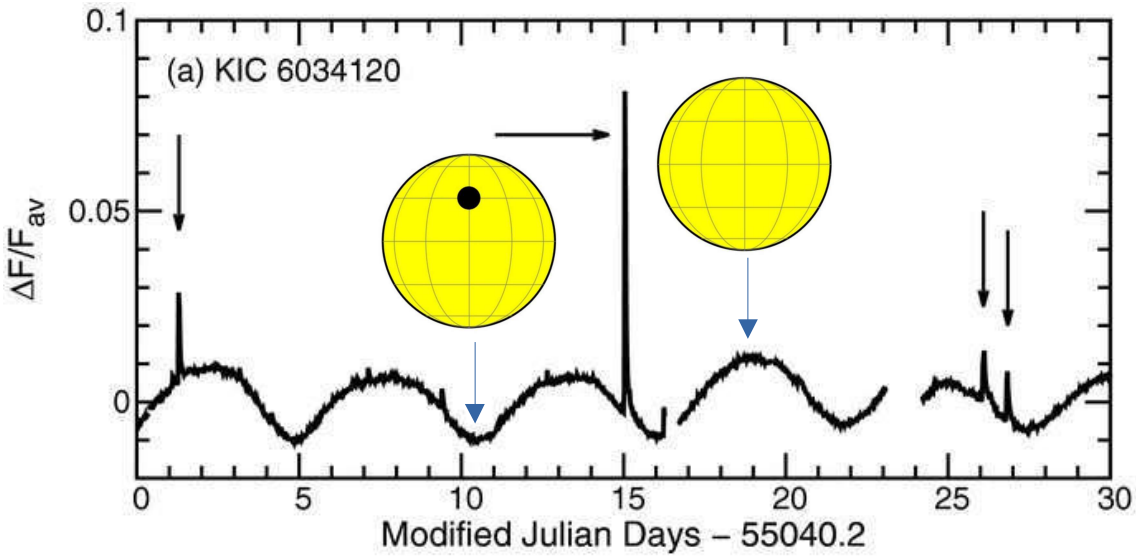


Figure 1.8: Kepler light curve of solar-type star (KIC 6034120), taken from Notsu et al. (2013), showing periodic brightness variations with respect to average brightness ($\Delta F/F_{av}$) caused by the rotation of starspots across the stellar disk. The black arrows mark the occurrence of superflares as reported by Maehara et al. (2012) and blue arrows show the position of starspots on the stellar disk through the light-curve modulation. (Image Credit: Notsu et al. (2013))

### 1.3.2 Chromospheric Activities

Chromospheric activity in stars encompasses magnetic phenomena like plages, spicules, flares, and heating, linked to the magnetic fields and dependent on stellar properties. These activities are traced using spectral lines such as Ca II H & K, H$\alpha$, Mg II h & k, and the Ca II infrared triplet, which exhibit emission due to the non-thermal heating (Hall, 2008). Different lines probe varying chromospheric depths; Ca II lines indicate mid to lower chromosphere activity, while H$\alpha$ reflects upper chromospheric and flare emissions. The Ca II H & K line cores are key indicators of the magnetic heating, quantified by the S-index (Vaughan et al., 1978) and the photospheric-corrected $R^{'}_{HK}$ index for the better representation of chromospheric activity in stars (Noyes et al., 1984a). These diagnostics enable the identification of the activity cycles and classifications of the stars in active and inactive groups as seen in the Mount Wilson HK survey. High-resolution observations across the UV to IR spectrum have further helped in modeling stellar chromospheres, and these observational studies confirm chromospheric activity across various stellar types, including binaries and late-type stars, highlighting the utility of these diagnostics in tracing stellar magnetism.

### 1.3.3 Coronal Activities

The corona is a host to some of the most dramatic and energetic transient phenomena. Coronal activity encompasses a variety of dynamic processes, including prominences, filaments, flares, jets, and coronal mass ejections (CMEs), all of which are governed by the magnetic field. In both the Sun and Sun-like stars, these phenomena represent energy release events linked to the magnetic reconnection or instabilities in the coronal magnetic structures. In this thesis, while a brief overview of multiple coronal features is provided, our primary focus remains on the flares and CMEs, their temporal and spectral signatures,

and how they inform us about stellar magnetic fields and physical properties of the localized coronal structures. Some of the coronal activity indicators are outlined below:

#### 1.3.3.1 Filaments

Filaments are large, thread-like structures made of relatively cool and dense plasma that are suspended in the hot solar or stellar corona. They appear as dark, elongated features when observed against the bright solar disk in the chromospheric spectral lines such as H$\alpha$, and glow brightly when viewed off the limb, known as the prominences (Parenti, 2014). They form along polarity inversion lines in the photospheric magnetic field and remain stable through a balance of magnetic pressure and tension. However, this balance can be disrupted by processes such as magnetic reconnection or instabilities (Chen, 2011), leading to filament eruptions. These eruptions are often precursors to or directly associated with the solar flares and/or coronal mass ejections.

#### 1.3.3.2 Coronal mass ejections (CMEs)

CMEs are large-scale expulsions of plasma from the solar or stellar corona into the heliosphere or interstellar medium. CMEs generally exhibit a structure with three parts: a bright leading front, a dark cavity, and a bright core often associated with the erupting filament (Hundhausen, 1999; Webb and Howard, 2012). The speed of solar CMEs can vary from a few km/s to over 3000 km/s, with kinetic energies in the range of $10^{27-32}$ erg. CME mass estimates lie between $10^{13-16}$ gm, and their propagation can be categorized into accelerating, decelerating, or constant speed types, depending on the interplay of propelling and retarding forces (Gopalswamy et al., 2005; Gopalswamy, 2006). However, in the case of stellar CMEs, the kinetic energy and the mass of the ejected material are found to be 100 to 1000 times greater than those observed in solar CMEs (e.g. Karmakar et al., 2022).

#### 1.3.3.3 Solar flare

Solar flares are among the most dynamic and energetic phenomena in the solar atmosphere, characterized by sudden bursts of radiation across multiple wavelengths as shown in Fig. 1.9. The first ever observation of a solar flare was recoeded by Richard Carrington in 1859, who noted brightening near the sunspots, now known as white-light flares (Carrington, 1859). With the advancement of H$\alpha$ filters, two bright ribbon-like structures were detected in the chromosphere during the flares (Svestka, 1976). Subsequent discoveries of coronal radio and X-ray emissions confirmed that flares originate in the corona rather than in the lower solar atmosphere. Identification of the Sun's magnetic field (Hale, 1908) and advancements in soft X-ray telescopes established that magnetic fields serve as the primary energy source for solar activity, including flares.

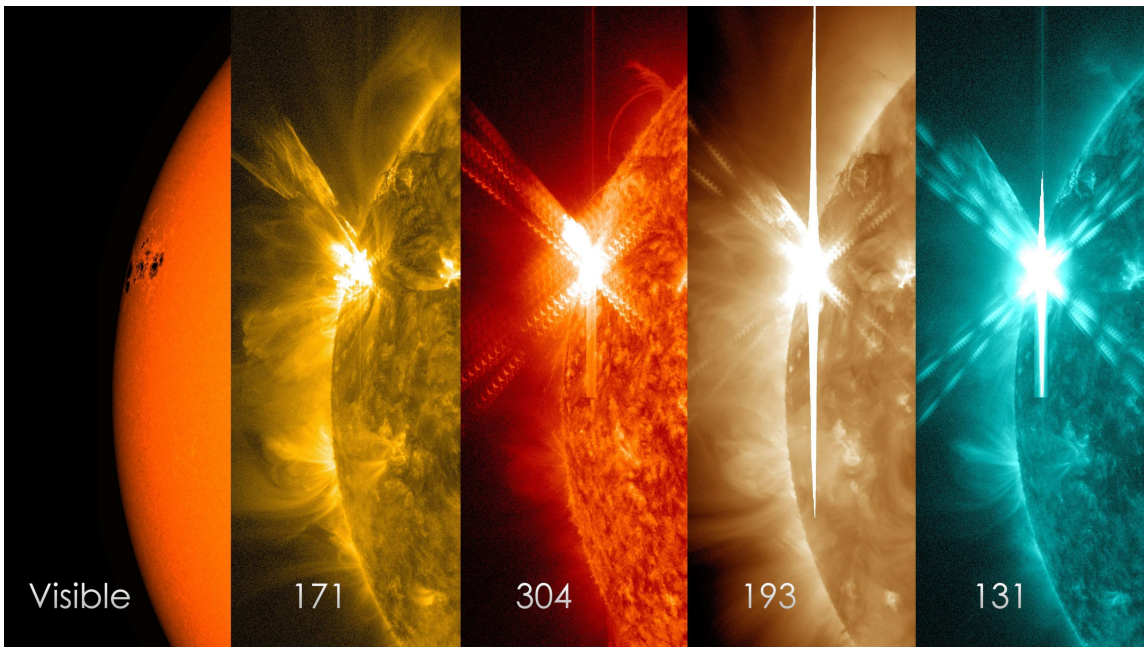


Figure 1.9: A solar flare observed on May 5, 2015, by the NASA's Solar Dynamics Observatory (SDO) is shown in multiple wavelengths of extreme ultraviolet light, each revealing plasma at different temperatures. From left to right, the images display visible light, followed by emissions at 171, 304, 193, and 131 Å. (Image Credit: NASA/GSFC/SDO)

Today, solar flares are understood as the result of sudden reconfigurations of the Sun's magnetic field through a process known as magnetic reconnection (Pontin and Priest, 2022; Priest, 2014), as discussed in detail in section 1.3.3.4. This rapid release of stored magnetic energy leads to an intense radiative emission and is often accompanied by a CME, which expels high-energy plasma into space. Flares typically originate from the active regions associated with the sunspots, and exhibit key observational features such as flare ribbons, footpoints, and post-flare loops (Aschwanden, 2002; Benz, 2008, 2017; Fletcher et al., 2011). Flare ribbons, visible in the H$\alpha$ and ultraviolet (UV) wavelengths, trace the magnetic field configuration and mark the regions where accelerated particles precipitate into the lower atmosphere. Footpoints, located at the bases of the coronal loops, serve as sites where non-thermal electrons produce hard X-rays via bremsstrahlung. As the flare evolves, post-flare arcades form, further emitting high fluxes of soft X-rays, signaling the gradual cooling and relaxation of the magnetic field.

The occurrence of solar flares is strongly linked to the sunspot activity, with larger sunspot areas storing greater amounts of magnetic energy. Even minor disturbances can destabilize these regions, increasing the probability of flare events. The energy output of the solar flares can reach up to $10^{32}$ erg, making them significant drivers of space weather and influencing planetary magnetospheres (Emslie et al., 2012; Fletcher et al., 2011). Solar flares are classified based on their energy release and X-ray flux in the 1–8 Å wavelength range, as observed by the Geostationary Operational Environmental Satellite (GOES). The classification consists of five main categories as shown in Table 1.2. In addition to the X-ray flux, flares can be classified into various types, such as impulsive (short, intense bursts of energy) or gradual (longer duration with fewer high-energy particles). Another distinction is between confined or compact flares, which remain restricted by the strong magnetic fields with no eruption, and eruptive (two-ribbon) flares, which are often linked to the CMEs and prominences (Pallavicini et al., 1977; Priest, 2014).

| Flare Class | X-ray Flux (1–8 Å, W/$m^2$) |
|---|---|
| A | $< 10^{-7}$ |
| B | $10^{-7}$ to $10^{-6}$ |
| C | $10^{-6}$ to $10^{-5}$ |
| M | $10^{-5}$ to $10^{-4}$ |
| X | $> 10^{-4}$ |

Table 1.2: Classification of the flares based on the peak X-ray flux in the wavelength range 1–8 Å (Harra et al., 2016).

#### 1.3.3.4 Magnetic reconnection

Magnetic reconnection is a fundamental process in the solar/stellar corona that enables the release of stored magnetic energy through topological changes in the magnetic field structure. The continuous generation of the magnetic flux by the solar dynamo, combined with differential rotation and convective motions, leads to the buildup of magnetic stresses in the corona. To alleviate this stress, the large-scale coronal magnetic field undergoes restructuring, resulting in the magnetic reconnection as shown in Fig. 1.10. This process occurs in the regions of intense magnetic complexity, such as twisted loops, filaments, and sheared neutral lines, where oppositely directed magnetic field lines break and reconnect and convert magnetic energy into the plasma heating, particle acceleration, and bulk plasma motions. Magnetic reconnection operates in different regimes, including steady 2D models, which provide basic analytical insights but oversimplify real flare conditions. The bursty 2D reconnection, which involves instabilities like the tearing-mode instability to explain the rapid energy release observed in the solar flares, and 3D reconnection models are necessary to account for more complex scenarios in understanding the dynamics of flares and coronal mass ejections (CMEs) (Priest, 2014). This process occurs across different solar regions, from magnetic flux emergence in the chromosphere to the microflares and large-scale eruptions in the corona, making it a crucial driver of the solar activity. To explain the observable features of solar flares, several models on the magnetic reconnection were introduced by Carmichael (1964), Sturrock (1966), Hirayama (1974), and Kopp and

Pneuman (1976). Despite being developed independently, these models share a broadly similar magnetic field configuration and dynamic evolution, and are collectively referred to as the CSHKP (Carmichael, Sturrock, Hirayama, and Kopp & Pneuman) model. This model is a standard model of flares, and its basic features are explained in the following section.

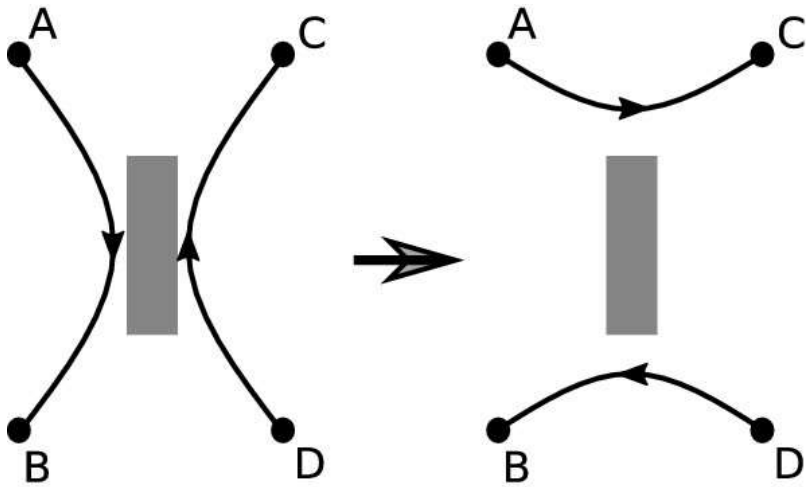


Figure 1.10: A change in magnetic topology in a localised diffusion region (shaded) produced by the magnetic reconnection is shown. A plasma element 'A' is initially connected to a plasma element 'B', which gets connected with element 'C' after reconnection. (Image Credit: Pontin and Priest (2022))

#### 1.3.3.5 Standard solar flare model

The standard solar flare model, also known as the CSHKP model, describes the formation and evolution of the solar and stellar flares. According to this model, flares originate when twisted magnetic field lines break and reconnect, releasing the stored magnetic energy, a process known as magnetic reconnection as discussed in section 1.3.3.4 (Kopp and Pneuman, 1976; Tsuneta et al., 1992). This occurs in the lower corona, where stored non-potential magnetic energy is rapidly converted into the kinetic energy, thermal energy,

and particle acceleration. The reconnection process releases vast amounts of energy, triggering the flares. The energy released during reconnection accelerates charged particles, primarily electrons and protons, to relativistic speeds through mechanisms that are still not fully understood. As these non-thermal electrons and ions move along the magnetic field lines, they spiral due to the Lorentz force, undergoing gyro-synchrotron emission. This motion produces intense radio waves, which are observed during the early phases of the flare. Some accelerated particles move downward along the closed magnetic loops and collide with the denser solar chromosphere at the footpoints of the flare loop. These electrons, traveling at nearly the speed of light, interact with the ions in the chromosphere through bremsstrahlung, emitting hard X-rays (Masuda et al., 1994, 1995). The hard X-ray emission closely follows the impulsive phase of the flare. The footpoints, now bombarded with the high-energy particles, heat up to extreme temperatures (millions of degrees) within seconds. This causes chromospheric evaporation, where the hot plasma expands upwards along the loop due to large pressure gradient. This rising plasma gradually fills the flare loops, leading to a steady increase in soft X-ray emission through thermal bremsstrahlung. The thermal component of the flare becomes dominant as the hot plasma cools down by the radiative and conductive losses. This cooling process emits soft X-rays and EUV radiation, marking the gradual decay phase of the flare. Fig. 1.11 illustrates the configuration of magnetic field lines in a 2D reconnection model.

Additionally, the time-integrated hard X-ray flux (non-thermal) is proportional to the soft X-ray flux (thermal), implying that non-thermal particle acceleration is directly responsible for the subsequent plasma heating, commonly known as the Neupert Effect (Neupert, 1968). When the chromospheric evaporation is efficient, it may significantly contribute to the coronal heating. Although large solar flares are not frequent enough to account for all coronal heating, a large number of small-scale flares (nanoflares) may play a crucial role (Parnell and Jupp, 2000). For deeper insight, advanced two- and

three-dimensional models have been developed to simulate these processes in greater detail (Moore et al., 2001; Priest and Forbes, 2002; Shibata et al., 1995; Shibata and Magara, 2011).

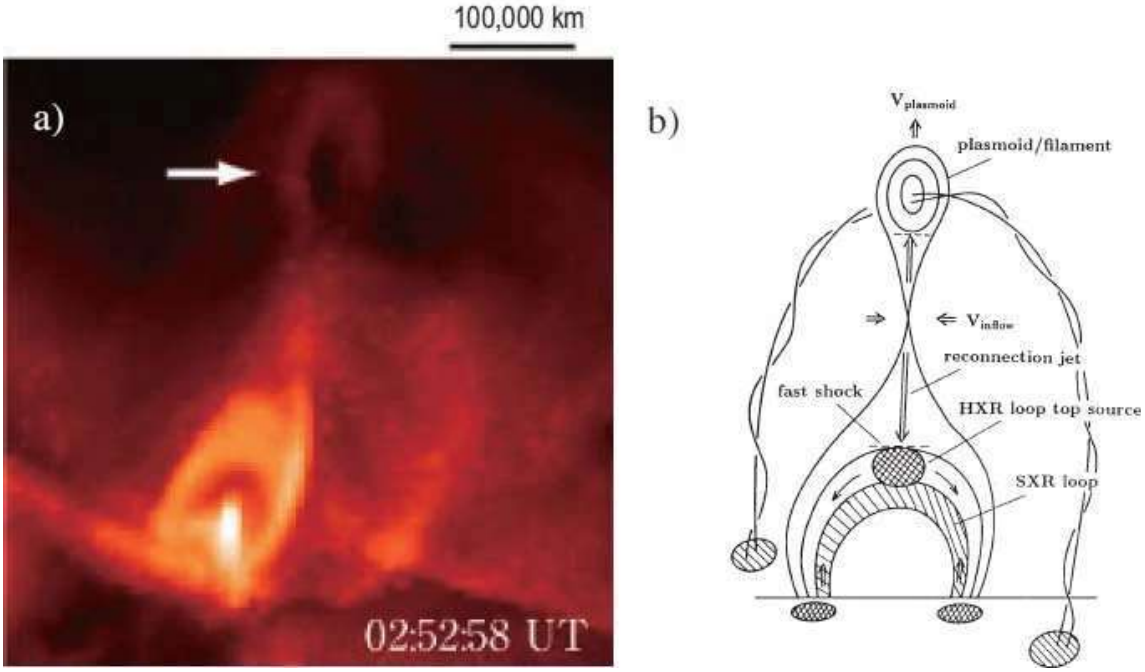


Figure 1.11: (a) Soft X-ray image of a long-duration solar flare captured by Yohkoh, (b) Schematic illustration of a modified CSHKP flare model adapted from Shibata et al. (1995); Shibata and Magara (2011).

#### 1.3.3.6 Stellar flares

Like the Sun, Sun-like stars exhibit flaring activity resulting from the dynamic behavior of their magnetic fields. However, in contrast to the solar observations, stellar flares are detected under spatially unresolved conditions, where stars appear as the point sources. These flares are identified by a sudden and prominent increase in stellar brightness in their light curves, often spanning multiple wavelengths. Such flaring events, driven by the magnetic reconnection in the stellar corona, are typically more energetic than the solar

flares. The flare frequency, duration, and intensity offer critical clues to the structure and evolution of stellar magnetic fields.

While classifications of solar flares exist (as discussed in section 1.3.3.3), applying these schemes directly to stellar flares requires caution. Unique stellar configurations such as complex magnetic fields, strong tidal interactions in close binaries, densely packed or polar magnetic fields, large-scale magnetospheres, or magnetic interactions with circumstellar disks in the pre-main-sequence stars can produce energy release mechanisms unlike those observed on the Sun. Stellar flares typically show rapid rise and slower decay, however, the EXOSAT flare survey revealed stellar flares exhibiting unusual morphologies, such as faster decays than rises, multiple peaks, and sudden flux drops (Getman et al., 2008; Haisch, 1983; Osten and Brown, 1999; Pallavicini et al., 1990; Reale et al., 2004). Such findings highlight the complex and diverse nature of stellar magnetic fields.

Missions like Kepler, TESS, and various X-ray observatories like Chandra, XMM-Newton, Astrosat, etc. have provided a wealth of data on flare characteristics across diverse stellar types. As highlighted in the solar flare models, flare features are prominently visible in the hard and soft X-rays. Hence, X-ray observations are essential for the comprehensive study of the stellar flares. The following sections delve into the observational signatures of stellar flares along with theoretical models developed to interpret and analyze these high-energy events.

#### 1.3.3.7 Flare observations

Observations of the stellar flares have significantly advanced our understanding of their properties and impact. Pallavicini et al. (1990) first analyzed flares in the solar-type stars using the X-ray data obtained from EXOSAT satellite, revealing a wide range of durations, structures, and intensities. van den Oord et al. (1988) categorized flares based on their rise times, suggesting that compact flares exhibit rapid rise times and involve one or a few small

loops, exhibit high plasma densities. However, longer rise time flares are likely two-ribbon events, involve large magnetic structures, and are associated with lower densities. A correlation between rise and decay times was later established by Osten and Brown (1999), who noted that flares with extended durations tend to have prolonged rise phases, with about 27% showing a double exponential decay. (Pandey and Singh, 2012) also showed that this characteristic was further supported by Favata and Schmitt (1999) and Favata et al. (2000), suggesting that morphological changes in the flaring regions contribute to this behavior. Observations of long-duration flares, such as those by Kuerster and Schmitt (1996) for CF Tuc and Maggio et al. (2000) for AB Dor, demonstrated that large coronal structures or polar flaring regions could result in visibility across a full stellar rotation. Additionally, Imanishi et al. (2001) detected a 6.4 keV neutral Fe fluorescent line in the flare spectra, indicating ionization effects on the interstellar medium (ISM). However, alternative sources such as photospheric or chromospheric fluorescence remain possible explanations. Changes in X-ray absorption column density can also indicate coronal mass ejections (CMEs) associated with the flares, leading to the variations in coronal abundances (Didel et al., 2024; Pandey and Singh, 2008; Tsuru et al., 1989). Highly energetic events known as superflares ($> 10^{33}$ erg) have been observed in stars such as AB Dor (Didel et al., 2024; Maggio et al., 2000), II Peg (Osten et al., 2007), Algol Favata and Schmitt (1999), CC ERI (Karmakar et al., 2017), and HR 1099 (Didel et al., 2025). These extreme events may be associated with CMEs, potentially influencing the stellar evolution and magnetic cycles. Superflares also play a crucial role in determining the habitability of exoplanets due to their intense radiation and particle flux (Lingam and Loeb, 2017), raising questions about the potential for similar occurrences on the Sun (Shibata et al., 2013).

Using these observations, detailed modeling of these flares provides significant insights into coronal heating processes and the morphology of the plasma structures. With adequate data from moderately time-resolved spectral observations, it is possible to trace the entire

flare evolution and derive critical properties such as, the dimensions of the flaring region or flaring loop length, the presence or absence of sustained heating during the flare, and constraints on the spatial distribution and location of the energy release (Reale et al., 2004). Over time, numerous loop models, often drawing on analogies with solar flares and built on varied assumptions, have been developed to interpret such phenomena as discussed in the following sections.

#### 1.3.3.8 Stellar flare models

The standard solar flare model provides a framework for understanding the mechanisms driving flaring activity and explains how the flare signatures manifest across the electromagnetic spectrum, as discussed in section 1.3.3.5. By utilizing multi-wavelength observations from various instruments, several theoretical models have been developed to explore stellar flares and their connection to solar flares. These models rely on analyzing flare light curves and spectra, incorporating heating and cooling processes inferred from both the observations and analogies with solar flares. Such detailed modeling has proven valuable in probing the coronal structures and magnetic field configurations of the stars, and each model offers distinct approaches to estimate parameters such as loop length, heating mechanisms, and plasma dynamics.

The attempt made by Haisch (1983) analyzed the stellar X-ray flares using the solar-like flare models assuming cooling through radiative and conductive processes, along with equality between decay time, radiative cooling time, and conductive cooling time at the flare maximum $\tau_{Decay} = \tau_{rad} = \tau_{cond}$,

$$\tau_{rad} = \frac{3K_B T}{n_e \Lambda(T)}, \quad \tau_{cond} = \frac{3n_e K_B L_{rad}^2}{\kappa T^{5/2}}. \tag{1.1}$$

Here, T is the loop temperature, $n_e$ is the electron density, $K_B$ is the Boltzmann constant, $\Lambda(T)$ is the plasma emissivity, $\kappa$ is the thermal conductivity, and $L_{rad}$ is the coronal loop

length. van den Oord and Mewe (1989) formulated an energy equation for cooling magnetic loops that mirrors the behavior of a static loop. They introduced a gradually decreasing heating rate, which balances energy losses on the star. Later, the quasi-static cooling model, proposed by Serio et al. (1991), assumes that the flare decay begins from a state where the loop is in hydrostatic and energy equilibrium. This model assumes the loop as semicircular with a constant cross-section, initially heated by an impulsive heat pulse. Once heating ceases, the loop cools through radiation and conduction. As a result, the loop evolves through a series of quasi-static states with progressively lower temperatures. The thermodynamic decay time ($\tau_{th}$) is derived in relation to the loop length ($L_9$: in units of $10^9$) as

$$\tau_{th} = \frac{120 L_9}{\sqrt{T_7}} \tag{1.2}$$

Reale et al. (1993) extended this model to include a gradually decreasing heating function and to accommodate loops of sizes comparable to or exceeding the pressure scale height. Further, the hydrodynamic loop model (Reale et al., 1997) accounts for the presence of continued heating during the decay phase, a factor not included in the quasi-static model. By analyzing the slope of the decay trajectory in the density-temperature (n–T) diagram, this model allows for a more accurate estimation of the loop length. The method incorporates both heating and cooling effects and derives relationships using the ratio of light curve decay time to the thermodynamic decay time.

$$\tau_{th} = \frac{120 L_9}{\sqrt{T_7} F(\zeta)}, \quad \text{Where} \quad F(\zeta) = \frac{c_a}{\zeta - \zeta_a} + q_a \tag{1.3}$$

Here, $F(\zeta)$ is the sustained heating factor and $\zeta$ is the slope of the density-Temperature (n-T) diagram. The constant parameters ($c_a$, $\zeta_a$, and $q_a$) tuned for different instruments are given in Table A.1 in Reale (2007). Further refinements were introduced by Reale (2007),

who extended the method to analyze both the rise and decay phases of a flare, providing complementary estimates of loop dimensions ($L_9$: in units of $10^9$ cm).

$$L_9 = 950 \frac{T_0^{5/2}}{T_M^2} t_M \tag{1.4}$$

Here, $T_0$ is the maximum flare temperature, $T_M$ is the temperature at the maximum density phase, and $t_M$ is the time at which the density maximum occurs.

The magnetohydrodynamic (MHD) model, introduced by Shibata and Magara (2011), focuses on the interplay between magnetic reconnection-driven heating and chromospheric evaporation. This model assumes that to maintain stable flare loops, the plasma pressure must remain below the magnetic pressure. It provides formulae to estimate loop length and magnetic field strength based on the emission measure, plasma density, and temperature.

Another important model is the two-ribbon flare model, which was initially developed for solar flares and later adapted for the stellar flares (Poletto et al., 1988). This model describes a process where an arcade of magnetic loops reconnects progressively at increasing altitudes, forming a system of growing loops. The associated magnetic energy release provides sustained heating, producing the observed X-ray emission. The geometry of the loop arcade is described using Legendre polynomials, and the time-dependent growth of the reconnection point is basically characterized by specific scaling relations.

All these models have been applied on stellar flares for comparative studies on different active stars: See Favata et al. (2000); Karmakar et al. (2022); Sasaki et al. (2021) for quasi-static cooling model, Didel et al. (2024, 2025); Karmakar et al. (2017) for hydrodynamic loop model, Pandey and Srivastava (2009); Poletto et al. (1988) for 2-Ribbon flare model, and Güdel (2004) for more details on flare models.

Among these, the hydrodynamic model, with its capacity to incorporate both heating and cooling during flare decay, remains one of the most robust and widely applied techniques. Consequently, in this thesis, flare loop modeling has been performed using the

hydrodynamic approach to obtain reliable estimates of stellar flaring structures using the rise phase and decay phase of the flare separately.

#### 1.3.3.9 Flare-CME relationship

Flares are often closely linked with the CMEs, especially during the large eruptive events, and both phenomena are believed to originate from a common underlying magnetic process through reconnection (Temmer et al., 2010; Švestka, 2001). While the Sun, despite being magnetically less active than many solar-type stars, frequently hosts such events, the scale of activity in younger, faster-rotating stars is expected to be significantly more intense (Donati et al., 1999; Strickert et al., 2024). Observationally, the direct detections of stellar CMEs remain difficult, but indirect evidences such as blueshifted emission lines (Argiroffi et al., 2019), Doppler-shifted Balmer profiles (Vida et al., 2019), and coronal dimming in EUV/X-ray bands (Veronig et al., 2021) support their presence. Notably, Veronig et al. (2021) identified five dimming events on the Sun-like star AB Dor, including a 13.3-hour EUV dimming consistent with a high-latitude CME. The persistent visibility of the dimming, given AB Dor's 0.51-day rotation period and inclination, suggests an origin in the polar active regions. However, strong global magnetic fields in such active stars could inhibit CME escape unless the eruptive energy is exceptionally high. Moschou et al. (2017) and Didel et al. (2024) reported a possible method for detecting stellar CMEs through variations in hydrogen column density ($N_H$). A transient increase in $N_H$ during a flare is interpreted as evidence of additional absorbing material, likely associated with an eruptive CME event crossing the line of sight. Thus, understanding the flare–CME connection in solar analogs not only helps in extending solar physics to stellar contexts but also provides insights into the energetic extremes possible in stellar magnetospheres. In the next Section 1.4, we describe observational diagnostics of superflares observed in X-rays.

## 1.4 Observational Diagnostics of Stellar Flares

Stellar light curves and X-ray spectra serve as crucial tools for diagnosing flares and probing the physical conditions in the stellar coronae. Even without spatial resolution, these observations can reveal important properties such as magnetic loop geometry, plasma temperature, emission measure, elemental abundances, and possible signatures of eruptive events. The detailed analysis of the flare evolution using light curves and abundance study using spectra is presented in the subsequent chapters.

### 1.4.1 Stellar Light Curve

The X-ray light curve of a star typically consists of two main components: the quiescent phase and the flare phase. The quiescent phase represents the baseline level of X-ray emission when the star is not undergoing any flaring activity. The quiescent phase represents the steady-state coronal emission arising from the relatively stable magnetic structures and is characterized by a relatively constant and low count rate. In contrast, the flare phase is observed as a sudden and transient increase in the X-ray emission above the quiescent state, signaling a magnetic energy release event in the stellar corona. The flare light curves can be further divided into three key segments as shown in Fig. 1.12.

The rise phase is the initial part of the flare where the X-ray flux rapidly increases due to the sudden heating of the plasma from the magnetic reconnection. It reflects the impulsive release of energy and the acceleration of the particles. The peak phase is the point where the X-ray flux reaches its maximum value. It represents the moment of maximum heating and plasma density in the flaring loop due to the chromospheric evaporation. The decay phase follows the peak phase, and the X-ray emission gradually declines as the plasma cools down through radiative and conductive processes. This phase can also reveal whether continued heating is present during the flare evolution.

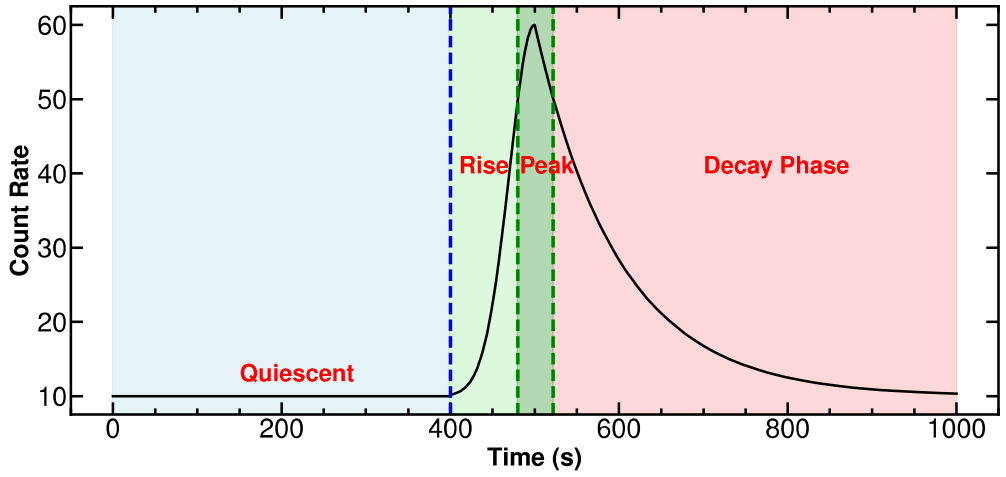


(A) Synthetic flare light curve

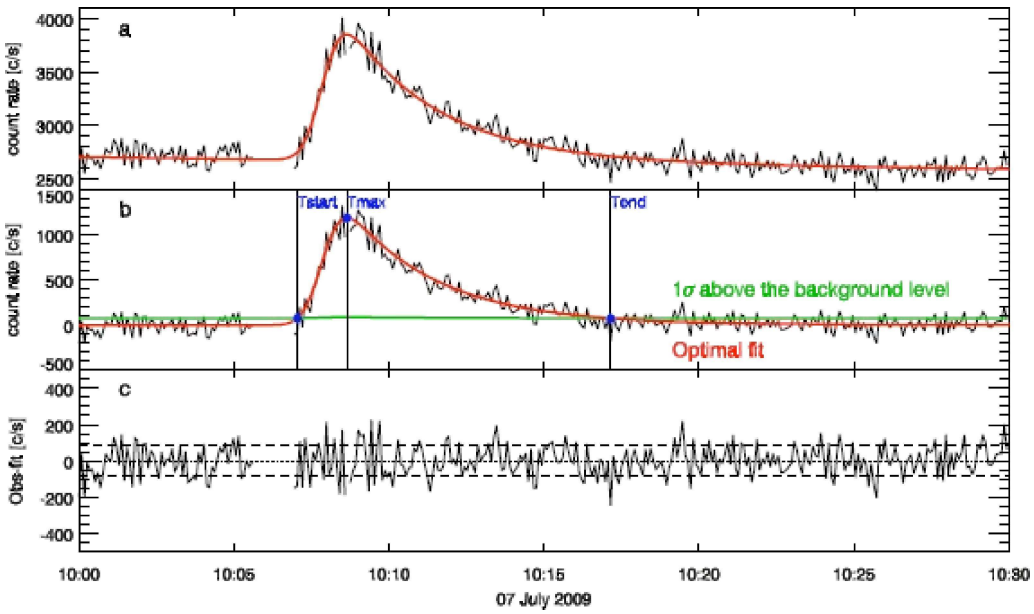


(B) Observed solar flare light curve

Figure 1.12: (A) The synthetic light curve displaying various segments, including the quiescent, rise, peak, and decay phases of a flare event. (B) An example of a solar flare light curve observed by SphinX spacecraft in the energy range 1.2 - 15 keV is shown. Panel (a) and (b) show the before and after background subtraction light curve with the best-fit flare profile overplotted in red. Panel (c) shows the residual of the best fit. (Image Credit: Gryciuk et al. (2017))

The flare light curves are typically modeled using functions such as exponential, double-exponential, or Gaussian profiles, depending on the observed rise and decay timescales. Comprehensive discussions on the detailed characteristics of solar and stellar flare profiles are given in Gryciuk et al. (2017); Kuznetsov and Kolotkov (2021); Seli et al. (2025). In addition to flares, both short and long-term variations in the light curve can reveal stellar surface features like starspots through rotational modulation, or the presence of stellar companions through orbital modulation.

In addition, X-ray rotational modulation in the light curve arises due to the rotation of magnetically active regions in a star's corona, where hot plasma confined in magnetic loops emits X-rays. In solar-type stars, this modulation is often linked to starspots and their associated coronal structures. In the Sun, such modulation has been well documented, demonstrating how the evolving active regions influence the global X-ray output (Orlando et al., 2004). The motion of these spots modulates the overall brightness of the star as discussed in sub-section 1.3.1. Interestingly, in some pre-main sequence stars, optical and X-ray light curves show an anti-correlation, meaning cool spots reduce the visible brightness while the overlying hot corona enhances X-ray emission (Guarcello et al., 2019). Notable examples of stars exhibiting X-ray rotational modulation include AB Dor (Didel et al., 2024; Singh and Pandey, 2024), HR 1099 (García-Alvarez et al., 2003; Linsky et al., 1989), EK Dra (Gregory et al., 2006), CF Tuc (Schmitt et al., 1996), and many more (Flaccomio et al., 2005; Marino et al., 2003). These studies underline the strong connection between surface magnetic features and coronal X-ray variability in both the Sun and active stars.

### 1.4.2 High-resolution X-ray Spectroscopy

The launch of advanced X-ray instruments revolutionized stellar coronal studies by providing high-resolution X-ray spectroscopy. These instruments record a rich array of discrete

spectral lines that can be individually resolved and analyzed, allowing precise determination of emission-measure distributions, elemental abundances, and electron densities. These spectra highlight the key features that reveal the underlying thermal structure of stellar coronae. From these line diagnostics, we can extract coronal abundances and, in turn, investigate how elements are fractionated as they move from the photosphere into the outer atmosphere.

#### 1.4.2.1 FIP and inverse-FIP effect

The elemental composition of the solar corona differs significantly from that of the underlying photosphere, a phenomenon first identified by Pottasch (1963). This difference, known as the First Ionization Potential (FIP) effect, describes the overabundance of low-FIP elements (FIP $\leq$ 10 eV) such as Mg, Si, and Fe in the corona relative to their photospheric values, typically by a factor of 3–4 (Feldman, 1992; Schmelz et al., 2012). In contrast, high-FIP elements like O, Ne, and Ar remain relatively unaffected or are sometimes depleted (Feldman and Laming, 2000; Feldman and Widing, 2003; Schmelz et al., 2012). The strength of this effect can be measured by a quantity "FIP Bias". It is defined as the logarithmic difference in the individual elemental abundance of low and high-FIP elements in the corona, compared to the photosphere ($log(X/H)_{photosphere} - log(X/H)_{corona}$). The solar observations have shown that the degree of FIP bias varies across different solar regions. The quiet coronal areas exhibit a modest FIP bias of 1–2, whereas active region loops develop a stronger bias of 3–4 as they evolve (Baker et al., 2015; Widing and Feldman, 2001). The Sun-as-a-star observations indicate that FIP fractionation is strongly correlated with the solar cycle phase (Brooks et al., 2017).

Similar abundance anomalies have also been identified in the coronae of late-type stars (Drake et al., 1994; Laming and Drake, 1999; Laming et al., 1995). With the enhanced spectroscopic capabilities of the Chandra and XMM-Newton satellites, a larger sample of

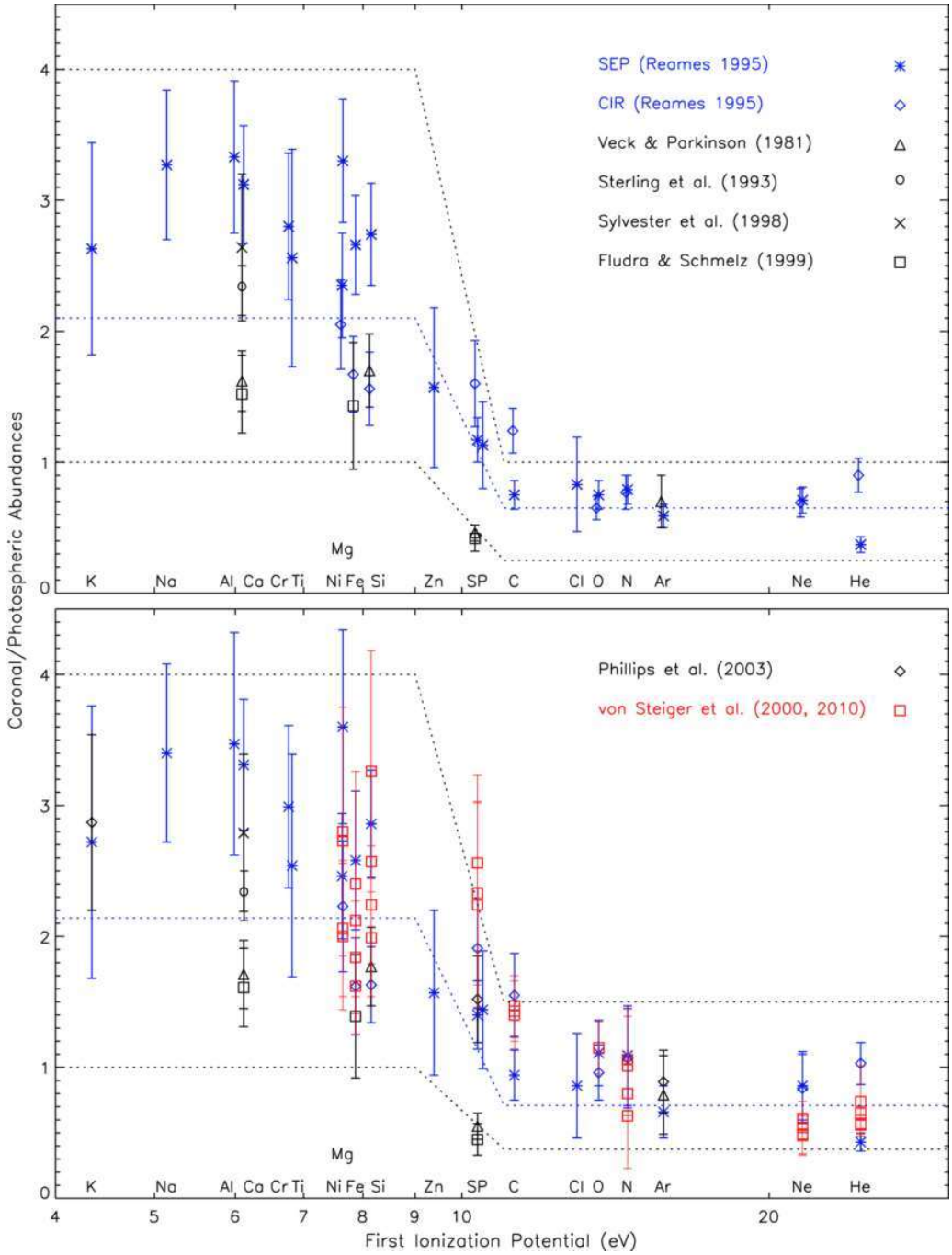


Figure 1.13: Solar coronal elemental abundances with respect to photospheric values are plotted against First ionization potential (FIP). The data is plotted from previous studies showing low-FIP abundance enhancement and high-FIP depletion with respect to photospheric values, or the so-called FIP effect. (Image Credit: Schmelz et al. (2012))

stellar coronae has been studied, revealing a correlation between the abundance anomaly and stellar spectral type. As shown by Wood et al. (2018), stars with spectral types earlier than or similar to the Sun exhibit a FIP-related coronal abundance anomaly. However, this effect diminishes for later spectral types, with coronal abundances approaching photospheric levels around mid-K-type stars. In even later spectral types, the anomaly reverses, leading to an "inverse FIP" effect, where low-FIP elements are depleted in the corona relative to the photosphere, reaching depletion levels of approximately 1/3 to 1/4 of the previously observed enhancement. Interestingly, patches of inverse FIP effect plasma have been observed in complex solar active regions (Baker et al., 2019; Laming, 2021). Baker et al. (2019) showed the evolution from the FIP to the I-FIP effect in patches above the flare ribbons, whereas the flaring loop apex showed an FIP effect. This suggests that the I-FIP effect can occur in the Sun under specific conditions, bridging the gap between solar and stellar observations.

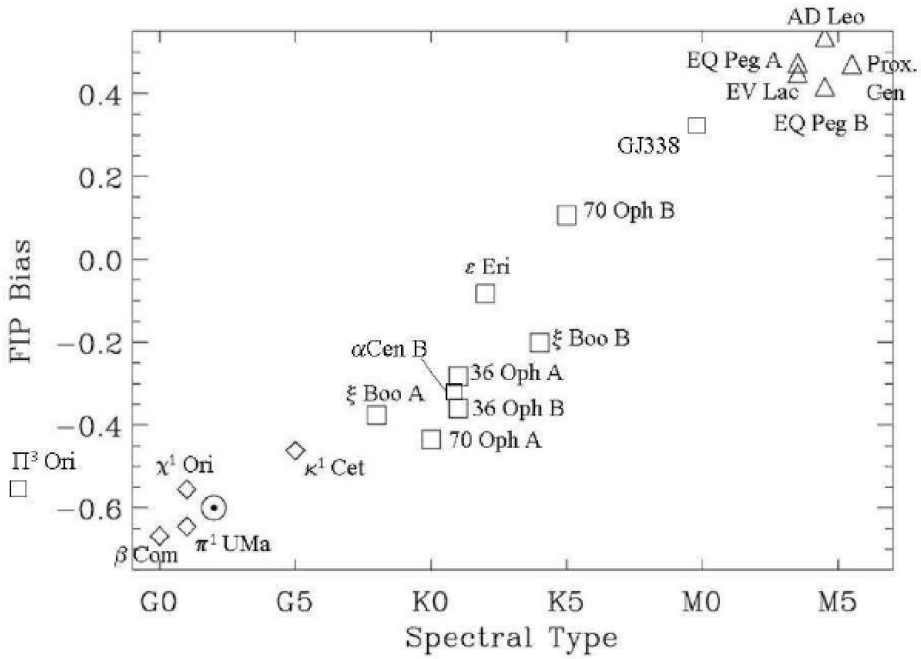


Figure 1.14: A graphical representation of FIP bias vs spectral type of the star from G0 to M5. (Image Credit: Wood and Linsky (2010))

In conclusion, the occurrence of FIP or inverse FIP effects depends on the spectral type and activity of the star. Solar-like stars generally exhibit the FIP effect, while more active stars, particularly M dwarfs, show the inverse FIP effect. This transition is likely related to the strength and geometry of the magnetic field, which tends to be stronger in later-type stars. The underlying mechanism of the FIP effect is believed to arise from ion-neutral interactions in the chromosphere, where low-FIP elements become preferentially ionized and transported into the corona via magnetic fields and wave-driven processes. The ponderomotive force fractionation model can account for both effects, depending on the properties of the waves and the coronal loop structure (Laming, 2004, 2015). These effects provide valuable insights into the processes of mass and energy transfer from the chromosphere to the corona in stars of various spectral types and activity levels. The abundance anomalies serve as important diagnostics for understanding solar and stellar coronal activities and underlying physical processes.

## 1.5 Aim and Objective of Thesis

The aim of this thesis is to investigate the coronal activities of a young and an evolved solar-type star, AB Doradus and HR 1099, respectively. The thesis is focused on the characteristics of the energetic X-ray flares and coronal loop geometry. Using XMM-Newton observations, this study aims to analyze the temporal variability of flare parameters and the spectral characteristics of these stars to understand the mechanisms governing their high-energy emissions. The objectives include characterizing flare parameters like temperatures, emission measures, and coronal elemental abundances using thermal plasma models, determining the loop lengths of the flaring structures, and comparing these properties with solar and stellar counterparts. A key aspect of this research is to explore the FIP and inverse FIP effects in the stellar coronae and examine their dependence on flare evolution and spectral type. By comparing coronal abundances of these stars with the

Sun and other late-type stars, this work aims to provide insights into the magnetic activity, coronal heating mechanisms, and plasma fractionation processes in the magnetically active stars. Furthermore, this study explores the possible connection between variations in hydrogen column density and signatures of failed eruptions or coronal mass ejections (CMEs), shedding light on mass-loss processes in the aforementioned active stars.

## 1.6 Outline of the Thesis

The first chapter, among the total seven chapters of this thesis, presents the introduction of the Sun and Sun-like stars, followed by an in-depth exploration of solar and stellar flares. It further considers the theoretical models describing the core mechanisms driving these intense magnetic activities.

*Chapter 2* discusses space-borne X-ray observations of the Sun-like stars and provides an overview of X-ray telescopes and detectors onboard the XMM-Newton observatory. It also discusses the data reduction process and spectral analysis tool XSPEC.

*Chapter 3* outlines examining the superflares detected on the rapidly rotating active star AB Doradus using X-ray observations. This investigates the presence of rotational modulation in the X-ray emission from the stellar surface caused by the starspots. A detailed analysis of the flare properties, including temporal evolution, spectral characteristics, and energy release, is presented. It also provides insights into the coronal loop geometry of this rapidly rotating star.

*Chapter 4* presents a study of superflares observed on the RS CVn binary system, V711 Tau, using time-resolved spectroscopy (TRS). Using data from XMM-Newton, the key flare parameters such as temperature, emission measure, and loop length were derived, providing insights into the coronal dynamics of this star.

*Chapter 5* explores the coronal plasma composition of two Sun-like stars, AB Dor and V711 Tau. By analyzing their elemental abundances relative to the solar photospheric

values, the presence of both FIP and inverse-FIP effects were identified, which explain the ion-neutral fractionation process in the magnetically active stars.

*Chapter 6* investigates X-ray flares in the active fast rotator AB Doradus, revealing a transient increase in hydrogen column density during the peak of multiple overlapping flares. The findings provide strong evidence for failed eruptions or coronal mass ejections (CMEs) associated with the flares. It offers a new approach for detecting such energetic plasma eruptions.

Finally, *Chapter 7* presents a summary of the key findings and conclusions, highlighting the significance of the original research carried out in this thesis. It also discusses potential directions for future studies.